Available online at www.sciencedirect.com
ScienceDirect
Journal of Sound and Vibration 324 (2009) 263–282
JOURNAL OF SOUND AND VIBRATION
www.elsevier.com/locate/jsvi

Structural stability of multi-folding structures with contact problem

Ichiro Ario[a,*], Andrew Watson[b]

[a]Department of Civil and Environmental Engineering, Hiroshima University, Higashi-Hiroshima 739-8527, Japan
[b]Department of Aeronautical and Automotive Engineering, Loughborough University, Leicestershire LE11 3TU, UK

Received 9 March 2007; received in revised form 22 January 2009; accepted 31 January 2009
Handling Editor: A.V. Metrikine
Available online 27 March 2009

Abstract

This paper presents the theoretical basis for both static and dynamic numerical approaches to the elastic stability of a folding multi-layered truss. Both analyses are based on bifurcation theory and include geometrical nonlinearity. The dynamic analysis includes an allowance for contact between nodes. Comparisons are made between published experimental folding patterns and the patterns obtained from both numerical methods in which bifurcations are demonstrated as elastic unstable snap-through behaviour. Several folding patterns are identified during the elastic instability where the folding behaviour of the truss is shown to be a function of the initial geometry and velocity of the dynamic loading. The authors suggest that the understanding of the behaviour will be very useful for the development of light weight structures subject to dynamic loading based on the bifurcation static analysis and dynamic analysis (using both the displacement control method and the load control method).

1. Introduction

There has been much work on the bifurcation analysis of structures using the general theory of elastic stability [1] in areas such as atomic structures and micro-truss structures, using the potential function. Hunt and Baker [2] invoke the Maxwell stability criterion based on global minima of energy in their examination of localisation in the fracture of brittle structures and elastic and dissipative truss-like models with bilinear constitutive characteristics. Ikeda et al. [3] show that an atomic matrix cellular model can suffer from an explosion of unstable post-buckling states associated with an n-fold compound critical point. The atomic models are analysed in a block diagonal context making use of the local and global symmetries of the structures. The behaviour identified by Ikeda et al. [3] is for bifurcation of rigid bar models where nodes can displace.

This paper presents a theoretical approach to examine the elastic stability of a folding multi-layered truss model as shown in Fig. 1(a). The theoretical folding patterns obtained are compared to the actual patterns

*Corresponding author.
E-mail addresses: mario@hiroshima-u.ac.jp (I. Ario), a.watson@lboro.ac.uk (A. Watson).

0022-460X/$ - see front matter © 2009 Elsevier Ltd. All rights reserved.
doi:10.1016/j.jsv.2009.01.057

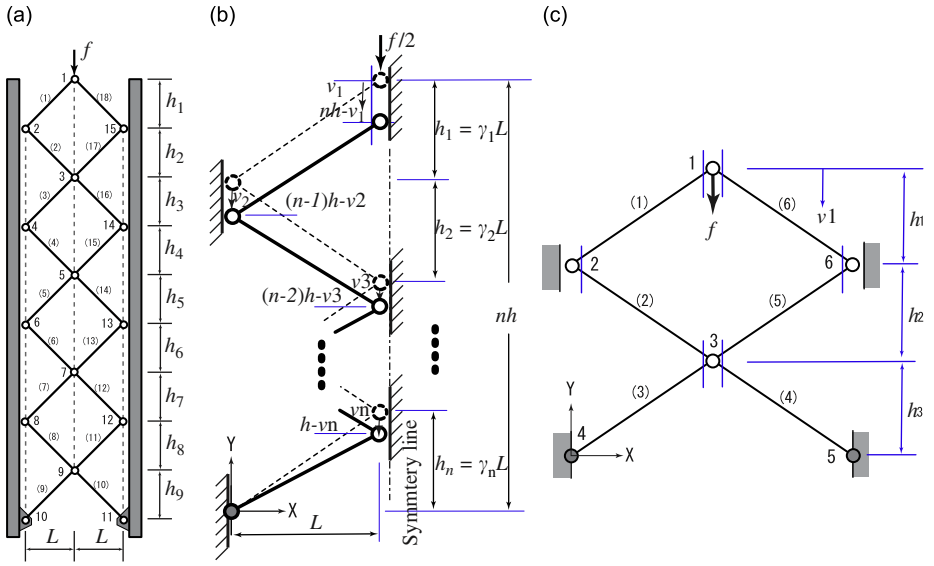

Fig. 1. Multi-folding pantographic systems: (a) multi-layer model, (b) one half of multi-layer model, (c) basic three layer model.

seen in the laboratory. The simplest truss has one layer and two elements and is better known as the Von Mises truss. The (shallow) truss has zero stiffness on the point of snap-through behaviour or unstable bifurcation phenomena allowing for geometrical nonlinearity [4–7]. Due to the complexity of the governing equations researchers have employed the finite element method to compute numerical solutions to model sequential snap-through behaviours in the folding and expanding truss with pantographic cells.

The instabilities shown by multiple layer, cellular and long structural systems have been investigated by other researchers. The review paper by Hunt et al. [8] investigates the cellular buckling that takes place in long structures with finite waves of localised buckles in sequence. The conclusions suggest a new explanation of the post-buckling behaviour of cellular structures with de-stiffening and re-stiffening characteristics. It is argued that the Maxwell load is the limit of the minimum energy localised solutions as end-shortening tends to infinity. If the structure were able to jump to the global minimum solution then the path for large displacement will become approximately flat at the Maxwell load.

The nonlinear equilibrium behaviour for both the static and dynamic analysis with contact problem are presented. The behaviour of the truss is different to that suggested by Hunt et al. [8]. Dynamic analysis with nodal contact results in different localised bifurcation modes. The truss model in this paper does not experience any horizontal motion of the nodes of the model. The layers are linked at nodes where there is load transfer anddisplacement continuity.

This paper presents a description of the general equilibrium of sequential instabilities and restabilities as a series of localised snap-throughs as an explanation for the experimental folding for a multi-layered pantographic truss.

In the field of smart structural engineering, Holnicki-Szulc et al. [9,10] put forward the concept of multi-folding micro-structures (MFM). In this work the problem of energy absorption under impact loading for multi-layered micro-structures was considered. For energy absorbing systems there are typically three requirements which are to: provide full dissipation of the kinetic energy; constrain excessive deformation; and to minimise the level of acceleration. Holnicki-Szulc et al. [9,10] carried out experiments to demonstrate the controlled folding of a three layered truss subject to impact loading and presented three different folding patterns. In this engineering issue, we have to consider elastic (in-)stability with several snap-through behaviours and a localised deformation, for example the number of snap-through behaviour in the system. In a previous paper the authors presented a numerical simulation with the top members of a three layered truss initiating the folding process [11], i.e. the members which were subject to the impact loading initiating the

folding process. This paper builds upon that work by presenting a generalised analysis of the multiple folding of a multiple layer truss and looking in detail at the folding behaviour of a three layer truss. I.e. folding behaviour initiated by any members in the multiple layer truss. Hence we present in this paper, the folding patterns for the system and derive a general formula for a truss with multiple layers shown in Fig. 1(a). The folding patterns of the three layer truss initiated by the top members presented in the previous paper [11] (see Figs. 6 and 7) are included. The multi-layered truss has right–left symmetry, hence in this paper the theoretical bifurcation analysis is limited to considering symmetric fold patterns. As such, by allowing for symmetric models only, we can therefore consider the half model shown in Fig. 1(b) for the theoretical analysis.

The bifurcation paths from the multiple singular point are found using bifurcation analysis. In this paper we establish multiple paths emanating from the initial compound bifurcation and limit point. In general, there is a difference between experimental behaviour and behaviour computed using 0-eigenvalue analysis for the singular stiffness matrix (e.g. see Ref. [12]). For static analysis it is shown that normal modes (approximate eigenvectors) depend on the geometrical nodal condition without eigenvectors from the nonlinear stiffness matrix.

The static and dynamic numerical simulations, of the basic truss shown in Fig. 1(c), each identify several folding patterns and these show good agreement with the experimental multi-folding behaviour. The numerical models allow for geometric nonlinearity and contact between nodes. To develop the numerical model the authors estimated the energy that initiates the multi-folding of the structure under impact. The experimental behaviour identified by Holnicki-Szulc et al. [9,10] was controlled by limiting the stress in an individual member and hence active control of the folding characteristics of the truss was achieved, resulting in the several different folding patterns in the experiment. For each of the different folding patterns the folding is initiated by a vertical impact load at the top node (i.e. node 1 in Fig. 1(c)). The model allows for symmetrical folding patterns only and therefore each node is restricted to have a vertical degree of freedom. (The authors do briefly discuss asymmetric folding in the paper.) The folding patterns of a multi-layered system are more complex and depend on the number of layers in the system. For the multi-layered model there are multiple snap-throughs identified after the initial bifurcation point (BP). The folding patterns can be controlled by introducing an imperfection to the position of the central node that displaces in the local snap through. The results show that for the three layer truss there are three different local folding patterns. The authors suggest that the understanding of the behaviour will be very useful for the development of light weight structures subject to dynamic loading based on the bifurcation static analysis and dynamic analysis (using both of the displacement controlling method and the load controlling method).

In his paper [13] on the snap through and snap back response of concrete structures Crisfield states that snap through involves a dynamic jump to a new displacement at a fixed load level. Snap back involves a dynamic jump to a new load level at a fixed displacement. In this paper the authors commit the offence of using the term snap through in both contexts.

2. Theory of elastic folding

In this section, we consider the folding mechanisms for the three layer truss structure subject to a vertical impact load at the top node shown in Fig. 1(c). The system is a pin-jointed elastic truss and all nodes of the system displace vertically only. No allowance is made for friction or gravity for this geometrically nonlinear problem.

2.1. Theoretical approach for multi-folding truss

We assume a periodic height for each layer of $h_i = \gamma_i L$ where the width L of the truss is fixed. Therefore, an initial length for each bar in the geometry of the figure is expressed as

$$\ell_i = \sqrt{L^2 + h_i^2} = L\sqrt{1 + \gamma_i^2} \quad \text{for } i = 1, \ldots, n. \tag{1}$$

The deformed length of each bar denoted as $\hat{\ell}_i$, is a function of the height and the nodal displacement variables

$$\begin{aligned}\hat{\ell}_1 &= \sqrt{L^2 + \{(nh - v_1) - ((n-1)h - v_2)\}^2} \\ &= L\sqrt{1 + (\gamma_1 - \bar{v}_1 + \bar{v}_2)^2}, \end{aligned} \tag{2}$$

$$\vdots$$

$$\hat{\ell}_i = L\sqrt{1 + (\gamma_i - \bar{v}_i + \bar{v}_{i+1})^2}, \tag{3}$$

$$\vdots$$

$$\hat{\ell}_n = L\sqrt{1 + (\gamma_n - \bar{v}_n)^2}, \tag{4}$$

where $\gamma_i = h_i/L > 0$, $\bar{v}_i = v_i/L$ $(i = 1, \ldots, n)$ and $\bar{v}_{n+1} = 0$ because the bottom node is translationally fixed.

Using Green's expression for strain (see Appendix A for engineering strain formulation) we obtain the elastic strain in each bar as

$$\varepsilon_i \equiv \frac{1}{2}\left\{\left(\frac{\hat{\ell}_i}{\ell_i}\right)^2 - 1\right\} \quad \text{for } i = 1, \ldots, n. \tag{5}$$

Substituting Eqs. (1)–(4) into Eq. (5) we obtain

$$\varepsilon_i = \frac{1}{2}\left\{\frac{1 + (\gamma_i - \bar{v}_i + \bar{v}_{i+1})^2}{1 + \gamma_i^2} - 1\right\} \quad \text{for } i = 1, \ldots, n. \tag{6}$$

The total potential energy, $\mathscr{V}$, of the half model, subject to loading $f/2$ is then given by

$$\mathscr{V} = \sum_{i=1}^{n} \frac{EA_i\ell_i}{2}(\varepsilon_i)^2 - \frac{f}{2}\bar{v}_1 L \tag{7}$$

$$= \sum_{i=1}^{n} \frac{EA_i L\sqrt{1+\gamma_i^2}}{2}\frac{1}{4}\left\{\frac{1 + (\gamma_i - \bar{v}_i + \bar{v}_{i+1})^2}{1 + \gamma_i^2} - 1\right\}^2 - \frac{f}{2}\bar{v}_1 L. \tag{8}$$

For the case when $\gamma_i = \gamma$ $(i = 1, \ldots, n)$ and $EA_i = EA$ $(i = 1, \ldots, n)$ the total potential energy can be written as

$$\mathscr{V} = \frac{\beta L}{8}\sum_{i=1}^{n}(\bar{v}_i - \bar{v}_{i+1})^2((\bar{v}_i - \bar{v}_{i+1}) - 2\gamma)^2 - \frac{f}{2}\bar{v}_1 L, \tag{9}$$

where the stiffness parameter $\beta = EA/(1+\gamma^2)^{3/2}$ (i.e. β is a function of γ). From Eq. (9), we can obtain the equilibrium equations based on the principal of minimum energy [1] in the following way:

$$F_i(\ldots, v_i, \ldots) \equiv \frac{\partial \mathscr{V}}{\partial v_i} = \frac{\partial \mathscr{V}}{\partial \bar{v}_i}\frac{\partial \bar{v}_i}{\partial v_i} = 0 \quad \text{for } i = 1, \ldots, n. \tag{10}$$

Hence, for the 1st, i-th and n-th equilibrium equations are

$$F_1(\bar{v}_1, \bar{v}_2) = \frac{\beta}{2}(\bar{v}_1 - \bar{v}_2)((\bar{v}_1 - \bar{v}_2) - \gamma)((\bar{v}_1 - \bar{v}_2) - 2\gamma) - \frac{f}{2} = 0, \tag{11}$$

$$\begin{aligned}F_i(\bar{v}_{i-1}, \bar{v}_i, \bar{v}_{i+1}) = {} & (\bar{v}_{i-1} - \bar{v}_i)((\bar{v}_{i-1} - \bar{v}_i) - \gamma)((\bar{v}_{i-1} - \bar{v}_i) - 2\gamma) \\ & - (\bar{v}_i - \bar{v}_{i+1})((\bar{v}_i - \bar{v}_{i+1}) - \gamma)((\bar{v}_i - \bar{v}_{i+1}) - 2\gamma) = 0, \end{aligned} \tag{12}$$

$$F_n(\bar{v}_{n-1}, \bar{v}_n) = (\bar{v}_{n-1} - \bar{v}_n)((\bar{v}_{n-1} - \bar{v}_n) - \gamma)((\bar{v}_{n-1} - \bar{v}_n) - 2\gamma) - \bar{v}_n(\bar{v}_n - \gamma)(\bar{v}_n - 2\gamma) = 0. \tag{13}$$

By using the implicit function theorem it is then possible to solve for all variables $\bar{v}_i$ $(i = n, \ldots, 1)$ as follows:

$$F_n(\bar{v}_{n-1}, \bar{v}_n) = 0 \rightarrow \bar{v}_n = \mathscr{F}_n(\bar{v}_{n-1}), \tag{14}$$

$$F_i(\bar{v}_{i-1}, \bar{v}_i, \bar{v}_{i+1}) = F_i(\bar{v}_{i-1}, \bar{v}_i, \mathscr{F}_{i+1}(\bar{v}_i)) = 0 \rightarrow \bar{v}_i = \mathscr{F}_i(\bar{v}_{i-1}), \tag{15}$$

$$F_1(\bar{v}_1, \bar{v}_2) = F_1(\bar{v}_1, \mathscr{F}_2(\bar{v}_1)) = 0, \tag{16}$$

where $\mathscr{F}(\cdot)$ denotes a nonlinear function. Thus we obtain all the solutions for each nonlinear equilibrium path by finding the normalised nodal displacements in turn.

The stability of the system is given by a nonzero value for the determinant of the tangent stiffness matrix, the *Jacobian* for $J \in \mathbf{R}^{n\times n}$. J is defined as follows:

$$J \equiv (J_{ij}) = \left(\frac{\partial^2 \mathscr{V}}{\partial v_i \partial v_j}\right) = \left(\frac{\partial^2 \mathscr{V}}{\partial \bar{v}_i \partial \bar{v}_j}\frac{\partial \bar{v}_i}{\partial v_i}\frac{\partial \bar{v}_j}{\partial v_j}\right) = \left(\frac{\partial F_i}{\partial \bar{v}_j}\frac{\partial \bar{v}_j}{\partial v_j}\right) \quad \text{for } i,j = 1,\ldots,n \tag{17}$$

and instability is defined as

$$\det J(v_i) = 0. \tag{18}$$

It is then possible to determine the buckling load and the post-buckling mode shape of the truss at the singular points from the nonlinear equations during instability.

2.2. Bifurcation analysis for three layers model ($n = 3$)

We now determine the equilibrium paths for the basic model shown in Fig. 1(c). The height of each layer is identical, i.e. $h_i = h$, hence $\gamma_i = \gamma$. In order to solve for the variable $\bar{v}_i$, we use the implicit function theorem and substitute $n = 3$ into Eqs. (13) and (14) which gives the solutions as follows:

$$\bar{v}_3 = \mathscr{F}_3(\bar{v}_2)\begin{cases} = \bar{v}_2/2 & \text{for primary path,} \\ = \frac{1}{2}(\bar{v}_2 \pm \sqrt{-3\bar{v}_2^2 + 12\gamma\bar{v}_2 - 8\gamma^2}) & \text{for bif. paths,} \end{cases} \tag{19}$$

$$\bar{v}_2 = \mathscr{F}_2(\bar{v}_1)\begin{cases} = 2\bar{v}_1/3 & \text{for primary path,} \\ = -\gamma + \bar{v}_1 \pm \frac{\sqrt{3}}{3}\sqrt{-(\bar{v}_1 - \gamma)(\bar{v}_1 - 5\gamma)} & \text{for bif. paths.} \end{cases} \tag{20}$$

The use of the implicit function theorem (16) and/or (11) for $\bar{v}_1$ leads to the following equation:

$$F_1(\bar{v}_1, \mathscr{F}_2(\bar{v}_1)) = f - \beta\mathscr{F}_1(\bar{v}_1) = 0 \tag{21}$$

hence it is seen that the relationship between the load parameter and the displacement $\bar{v}_1$ is nonlinear

$$f = \beta\mathscr{F}_1(\bar{v}_1). \tag{22}$$

Using $\bar{v}_2 = \mathscr{F}_2(\bar{v}_1)$ and $\bar{v}_3 = \mathscr{F}_3(\bar{v}_2)$ we can then express the equilibrium equations for the primary and bifurcation paths in terms of variable $\bar{v}_1$ as follows:

$$f_{\text{pri.}} = \beta\frac{\bar{v}_1}{3}\left(\frac{\bar{v}_1}{3} - \gamma\right)\left(\frac{\bar{v}_1}{3} - 2\gamma\right) \quad \text{for primary path,} \tag{23}$$

$$f_{\text{bif.}} = \pm\frac{\beta}{3\sqrt{3}}\sqrt{-(\bar{v}_1 - \gamma)(\bar{v}_1 - 5\gamma)}\cdot(\bar{v}_1 - 2\gamma)(\bar{v}_1 - 4\gamma) \quad \text{for bif. paths.} \tag{24}$$

The theoretical primary equilibrium and bifurcation paths are shown in Fig. 2(a) (see also Appendix B). We obtain the critical positions for the truss using the condition $\mathrm{d}f/\mathrm{d}\bar{v}_1 = 0$ for maximum and minimum values. For the equilibrium paths under consideration we obtain above the following result:

$$\bar{v}_1^{\text{BP}} = \frac{3 \mp \sqrt{3}}{3}(3\gamma) = (3 \mp \sqrt{3})\gamma = \begin{cases} 1.268\gamma \\ 4.732\gamma \end{cases} \quad \text{for } n = 3.$$

Finally, the maximum load is given by

$$f_{\max} = f(\bar{v}_1^{\text{BP}}) = \pm\frac{2\gamma^3}{3\sqrt{3}}\beta.$$

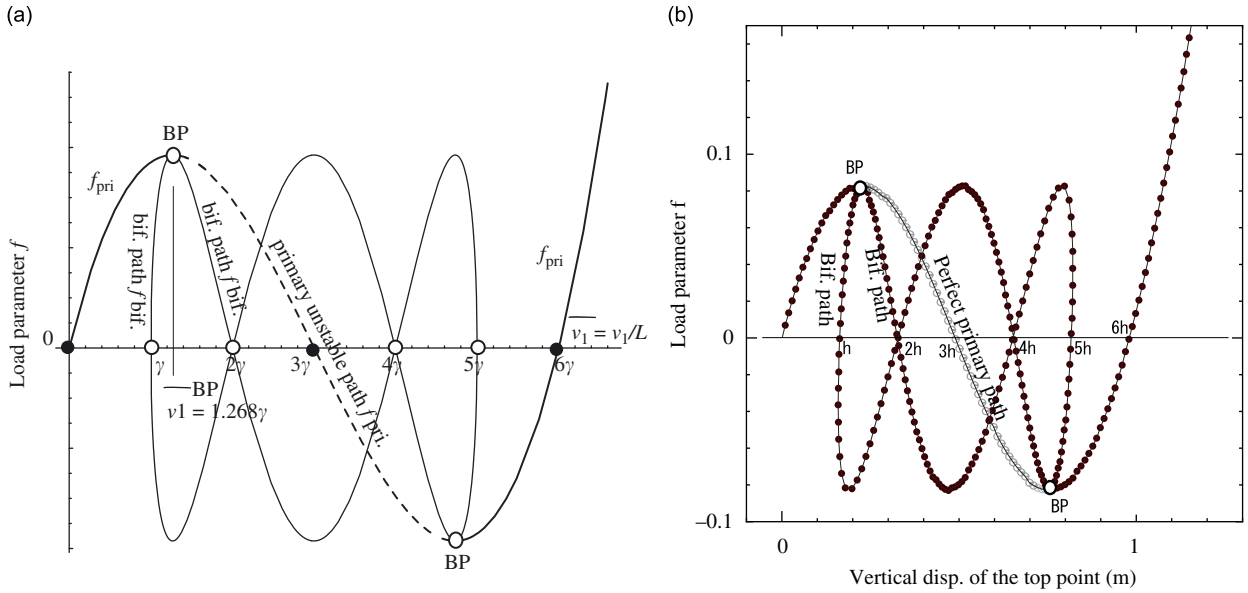

Fig. 2. Static equilibrium paths without contact for the basic model: (a) theoretical equilibrium paths using Eqs. (23) and (24), (b) numerical static equilibrium paths.

2.3. Numerical considerations for static analysis

The solutions to the static equilibrium equations (23) and (24) were found using the arc-length method [14–18]. These solutions identify the paths followed for each of the three folding patterns for the three layer truss and are shown in Fig. 2(a). Fig. 2(b) shows the corresponding numerical solutions. The different paths followed for the folding patterns of the truss start from the initial point of instability. This point indicated by BP in Fig. 2(a) and (b) is called the multiple BP and the maximum (or minimum) limit point. The eigenvalue at this singular point is zero. The results of the numerical analysis, i.e. the static equilibrium primary and bifurcation paths identified are shown in Fig. 2(b). The numerical results correspond approximately to the theoretical solutions shown in Fig. 2(a) (see also Fig. 15). The line of least stiffness after BP is that of the two bifurcation paths which means local snap-through (member folding) behaviour has occurred.

2.4. Folding modes

Ikeda et al. [3] show that an atomic matrix cellular model can suffer from an explosion of unstable post-buckling states associated with an n-fold compound critical point. The atomic models are analysed in a block diagonal context making use of the local and global symmetries of the structures and various kinds of localisation are identified for both unlinked and weakly linked models. The deformation modes of a single cell are examined in the paper and it is concluded, due to energy considerations, that for the unlinked model the most likely failure state is one of thorough localisation.

Two modes are identified for the single cell, namely mode A and mode B in Fig. 8 of that paper [3]. Group theory is used in the analysis for the description of the symmetries. Mode A and mode B are bifurcations which follow paths that deviate from the primary path. Mode A is an asymmetric mode and mode B is symmetric about a horizontal axis collinear with the loading.

The asymmetric deformation of the local folding of mode A is *a symmetry breaking path* that deviates from the primary path. For mode B occurring at the critical point B there are two paths separating: one is global folding D_2 and the other one is local symmetric folding D_1 mode.

There is similarity with the mode B of Ikeda et al. [3] where we have the right–left symmetry about a vertical axis which is collinear with the loading direction as D_1 in comparison with the up–down symmetry for the mode B. The number of different paths after the critical point B again should depend on the

number of cell (elements) or model layers. The physical significance of this being that there is one path for the different folding patterns based on the geometrical symmetry of a structure containing homogenous cells.

For the static problem the folding patterns can be found by considering the eigenproblem of the Jacobian. For the folding patterns that are identified no contact between nodes is assumed. Hence for the localised folding as shown below although the gap between nodes does reduce to zero no contact occurs.

For all singular paths at the BP the Jacobian equates to zero, i.e. when the increasing deformation $\bar{v}_1$ reaches a critical value $\det J = 0$. For the particular case when $\det J(\bar{v}_1^{\mathrm{BP}}) = 0$ of Eq. (18) three eigenvectors are obtained $\boldsymbol{\eta}_i$ and shown in Fig. 3.

The different collapse modes or folding patterns corresponding to these eigenvectors are shown in Fig. 3(a)–(c) as follows: (a) Eigenvector $\boldsymbol{\eta}_1$ shows localised folding of the top member. (b) Eigenvector $\boldsymbol{\eta}_2$ shows localised folding of the middle member. (c) Eigenvector $\boldsymbol{\eta}_3$ shows localised folding of the bottom member. These folding patterns are those identified by the bifurcation paths.

The vertical gap between nodes prior to loading is $2h$. During the folding process when nodes come into contact the vertical gap reduces to zero. In the following four subsections each of the eigenvectors shown in Fig. 3(a)–(c) are discussed. Because of symmetry of the folding pattern the discussion is limited to the left-hand half of the truss only. The static behaviour compares with the dynamic behaviour described below and behaviour observed in experiments as seen in Figs. 6, 8,12.

2.4.1. *Proportional deformation: global folding (primary path)*

The mode shape for this eigenvector shows proportional folding of all the members and corresponds to the primary unstable equilibrium path shown in Fig. 2(a). When the top node (node 1) has displaced by a vertical distance $3h$ then, due to proportional displacement of all nodes, all the members are horizontal. This corresponds to the point in Fig. 2(b) when the primary path graph crosses the horizontal axis at $3h$.

2.4.2. *Folding mode $\boldsymbol{\eta}_3$: localised folding initiated by bottom member (bifurcation path)*

The mode shape for this eigenvector corresponds to the bottom member folding shown in Fig. 3(c). When this members folds the gap between nodes 2 and 4 reduces to zero. For this fold pattern the members joining nodes 2 to 3 and 4 to node 3 will be collinear and adjacent.

2.4.3. *Folding mode $\boldsymbol{\eta}_2$: localised folding initiated by middle member (bifurcation path)*

The mode shape for this eigenvector corresponds to the middle member folding shown in Fig. 3(b). When this member folds the gaps between nodes 1 and 3 and nodes 2 and 4 reduces to zero. Hence for this fold pattern the members joining nodes 1 to 2, nodes 3 to 2 and nodes 3 and 4 will be collinear and adjacent (Table 1).

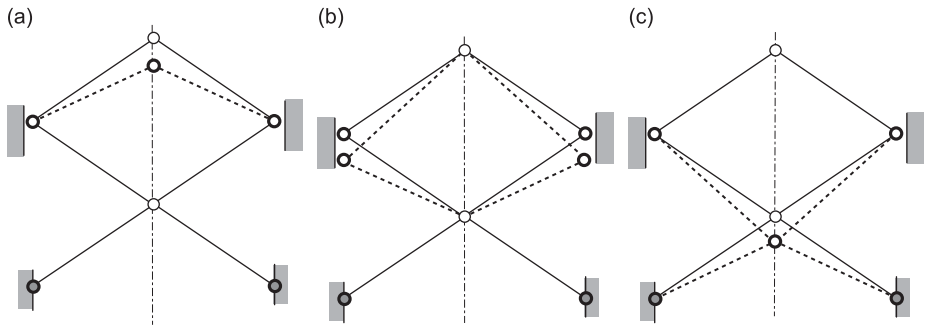

Fig. 3. Nodal displacement initiating fold mode: (a) the top members folding mode as $\boldsymbol{\eta}_1$, (b) the middle members folding mode as $\boldsymbol{\eta}_2$, (c) the bottom members folding mode as $\boldsymbol{\eta}_3$.

Table 1
Nodal initial position with perfect model.

Node	X (m)	Y (m)
1	0.240	0.489
2	0.000	0.326
3	0.240	0.163
4	0.000	0.000
5	0.480	0.000
6	0.480	0.326

Table 2
The coordinates of nodal points.

Node	X (m)	Y (m)
1	0.240	0.489
2	0.000	0.327
3	0.240	0.163
4	0.000	0.000
5	0.480	0.000
6	0.480	0.326

2.4.4. Folding mode $\boldsymbol{\eta}_1$: localised folding—top member (bifurcation path)

The mode shapes for these eigenvectors show similar behaviour and correspond to the top member folding shown in Fig. 3(a). When the top member folds the gap between nodes 1 and 3 reduces to zero. For these fold patterns the members joining nodes 1 to 2 and 3 to node 2 will be collinear and adjacent.

3. Dynamic analysis for folding truss allowing for contact

The dynamic analysis equation for the folding truss combines mass, damping and nonlinear stiffness $\boldsymbol{F}(\boldsymbol{v})$ in the following equation:

$$M\ddot{\bar{\boldsymbol{v}}}(t) + C\dot{\bar{\boldsymbol{v}}}(t) + \boldsymbol{F}(\bar{\boldsymbol{v}}(t)) = 0, \tag{25}$$

where $M \in \mathbf{R}^{N\times N}$ is the mass matrix; $C \in \mathbf{R}^{N\times N}$ is the damping matrix; $\boldsymbol{F}(\cdot)$ is the nonlinear stiffness vector; $\{\ddot{\bar{v}}_i(t)\}^{\mathrm{T}} = \ddot{\bar{\boldsymbol{v}}}(t) \in \mathbf{R}^N$ is normalised acceleration; $\{\dot{\bar{v}}_i(t)\}^{\mathrm{T}} = \dot{\bar{\boldsymbol{v}}}(t) \in \mathbf{R}^N$ is the velocity; $\{\bar{v}_i(t)\}^{\mathrm{T}} = \bar{\boldsymbol{v}}(t) \in \mathbf{R}^N$ is the normalised displacement and N is the total number of degrees of freedom in the system. If the mass and damping in this system are given as independent uniform variables $m_i = m,\ c_i = c\ (i = 1, \ldots, n)$, then we obtain the equation from Eq. (16) for the nodal variables $\ddot{\bar{v}}_1(t), \dot{\bar{v}}_1(t), \bar{v}_1(t)$ and this results in the following equation:

$$m\ddot{\bar{v}}_1(t) + c\dot{\bar{v}}_1(t) + F_1(\bar{v}_1(t), \mathscr{F}_2(\bar{v}_1(t))) = 0. \tag{26}$$

We solve this equation using the dynamic numerical method [5,6] with both incremental load and incremental displacement.

3.1. Numerical and contact conditions of the model

The nodes for the FEM model are shown in Fig. 1(c) and Table 2. The extensional stiffness of all members in the model have a normalised value of $EA = 1$. The value for geometric stiffness parameter β is given as

$$\beta = \frac{EA}{(1+\gamma^2)^{3/2}} = \frac{1}{(1+0.679^2)^{3/2}} = 0.566,$$

where $\gamma = h_1/L = \frac{0.163}{0.240} = 0.679$. For the contact problem we introduce an additional virtual element between nodes 1 and 3; nodes 2 and 4 (and nodes 6 and 5). We assume a constant level of damping, c, and mass, m, for all elements. We assume frictionless pins and zero gravity.

Using Eqs. (21) and (26) we obtain the dynamic equation for the displacement $\bar{v}_1(t)$ for node 1 as follows:

$$m\ddot{\bar{v}}_1(t) + c\dot{\bar{v}}_1(t) + (\beta\mathscr{F}_1(\bar{v}_1) - f) = 0, \tag{27}$$

dividing each term by m, we obtain the following equation:

$$\ddot{\bar{v}}_1(t) + c'\dot{\bar{v}}_1(t) + \beta'\mathscr{F}_1(\bar{v}_1) = f', \tag{28}$$

where $c' = c/m$, $\beta' = \beta/m$ and $f' = f/m$ (and includes both the primary path and the bifurcation loads). Therefore, this Eq. (28) includes explicit form of the function $\mathscr{F}_1(\cdot)$. If the value of the damping parameter c' is small, the system response appears as vibration motion analogous to a molecular model.

3.2. Criteria for contact condition during dynamic analysis

The analysis includes the virtual elements which allows for modelling the contact problem. The stiffness of the virtual members is nonzero when the length of the virtual member is zero (i.e. nodes are in contact). However, if the member length is greater than zero (i.e. no nodal contact) the virtual member contributes zero stiffness to the system stiffness. The length of the virtual member (termed dummy member hence) and associated axial stiffness is defined in the following equation:

$$\hat{\ell}_{\text{dummy}} \begin{cases} > 0, & EA_{\text{dummy}} = 0 \quad \text{without contact,} \\ = 0, & EA_{\text{dummy}} = 1000 \quad \text{with contact.} \end{cases} \tag{29}$$

During the folding process prior to any contact between nodes all dummy elements have zero stiffness since the lengths of these dummy elements are nonzero. At contact there is an increase in stiffness of the system. The individual stiffness of each (real) member is unchanged; however, due to an increase in system stiffness, caused by contacting nodes, a value of $EA = 1000$ for the dummy elements was found to give good results for the folding pattern behaviour of the pantographic truss.

The analysis allows for separation of nodes during the dynamic behaviour. As such the length of the dummy element, $\hat{\ell}_{\text{dummy}}$, can increase from zero. As soon as there is a gap between nodes the stiffness of the dummy element becomes zero again. Hence there is no 'extra stiffness' during any noncontact behaviour occurring after any contact behaviour. If local snap-through behaviour occurs there will be contact for the restabilised state.

For each of the folding processes shown in Fig. 3(a)–(c) contact occurs between nodes. When local folding is initiated by the top member this initially leads to contact between nodes 1 and 3. Further loading will eventually result in the bottom member folding and contact between nodes 2 and 4. When local folding is initiated by the bottom member there is contact between nodes 2 and 4. Further loading will eventually result in the top member folding and contact between nodes 1 and 3. For middle member initiated folding results in contact between nodes 1 and 3 plus nodes 2 and 4. For the primary path folding no contact occurs.

3.3. Folding processes by experiment and numerical simulation

We have developed a path following technique for the dynamic folding of a system under impact loads that allows for both load control and displacement control. The results of the numerical simulations are compared with the laboratory experiment carried out by Holnicki-Szulc et al. [10]. For each of the folding patterns initiated by local folding in the dynamic analysis the experimental and numerical results are described and compared. Six photographs of the experimental folding process are shown (A–F) where Picture (A) for each folding process is the initial location of the structural system prior to impact. In the experimental tests displacement at the joints is possible in the vertical direction only and the top joint is the point of application of the impact load. Each of the six members have identical properties of absolvers (stiffness). For the

numerical solutions an imperfection was added to the input data for each folding process to initiate the desired folding process by displacing the position of the node that initiates the folding process, by 1 cm (i.e. either node 1 (top member) or node 3 (for bottom or middle member)).

3.4. *Local folding initiated by bottom members for* (η_3)

The experimental behaviour showing the bottom members initiating the folding process is shown in Fig. 4. The numerical solutions and folding processes are shown in Fig. 5. The experimental behaviour is described as follows: Picture (A) in Fig. 4 shows the initial position of the system; Picture (B) shows the bottom members in the process of the first snap through and in an approximately horizontal state; Picture (C) shows the post-snap through of the bottom members; Picture (D) shows the top members during the second snap-through process and in an approximately horizontal state; Picture (E) shows the post-snap through of the top members. Picture (F) is the all contact state for all members. For the displacement control simulation the folding process is shown as (a)–(f) in Fig. 5(b). For the load control simulation the folding process is shown as (a), (d) and (f′) (at higher load). Hence there are two snap-throughs: first in the bottom members and then later in the top members for either approach.

For the displacement control simulation Fig. 5(a) shows at (a) (i.e. BP at the onset of instability) there is a sudden loss of stiffness and the path followed is shown as the black solid dots. After snap through of the bottom members there is local restabilisation and a positive stiffness. The line keeps climbing until (d) is reached which marks the onset of the second snap-through instability and the top members snap through. When restabilisation occurs no further snap through is possible and the system stiffness (measured as the gradient of the load displacement curve) keeps increasing to a new maximum value. When compared to the static paths the process after (b)–(d) are very similar. At (f) all the members are in contact. However after (f) the system stiffness is higher than the system stiffness on the static path (where there is no contact) and these paths separate. Hence the stiffness modulus has increased significantly contact takes place. For the load control simulation Fig. 5 shows the dynamic path followed as the row of horizontal gray dots. Hence the path followed is from (a) for the first snap through and (d)–(f′) as the second snap through. When restabilisation occurs no further snap through is possible and the system stiffness keeps increasing. The magnitude of the load f_{BP} for this pattern almost equals f_{d} and $f_{\mathrm{f'}}$.

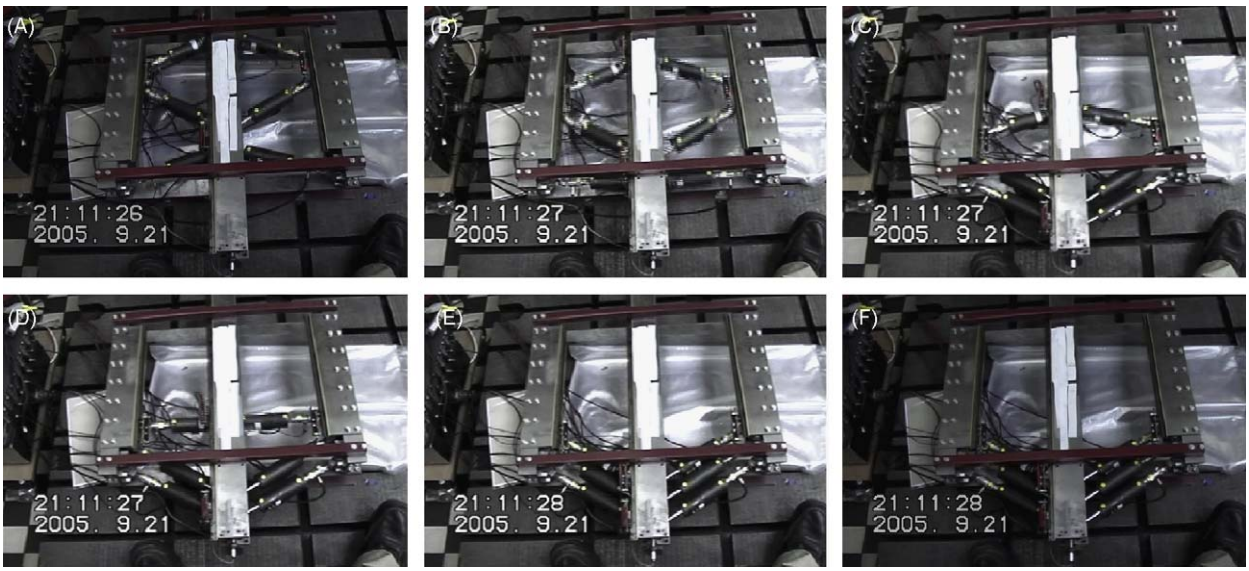

Fig. 4. Experimental behaviour showing bottom members initiating folding process from (A) to (F) (observed by J. Holnicki-Szulc and P. Pawłowski).

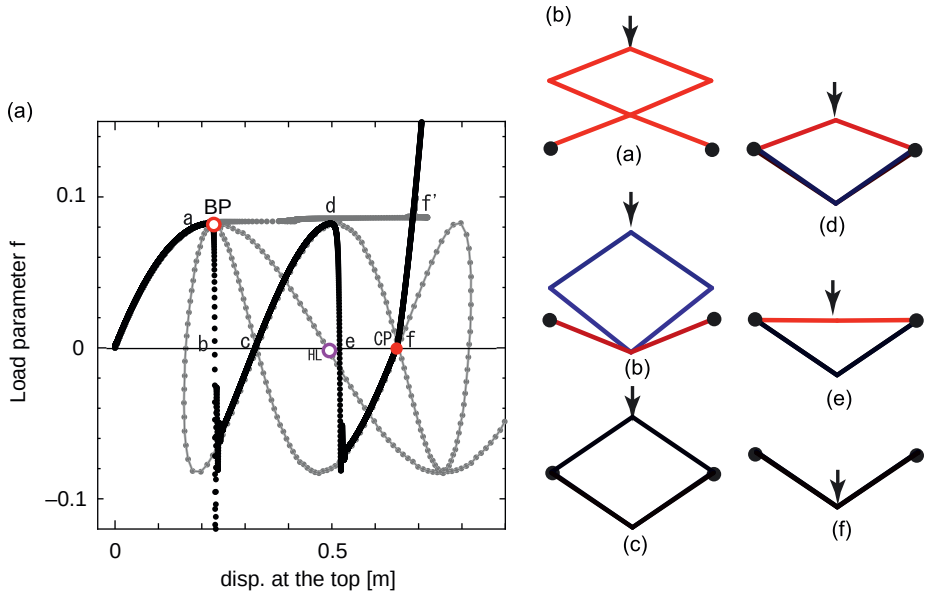

Fig. 5. Numerical solutions for bottom members initiating folding pattern: (a) dynamic and static equilibrium paths compared, (b) folding processes by the dynamic displacement control method. (The red colour indicates compressive stress and blue colour indicates tensile stress. Abbreviations used in this figure and below HL and CP where HL—horizontal line: position when all members are horizontal; CP—contact point: members are in contact) (For interpretation of the references to colour in this figure legend, the reader is referred to the web version of this article.).

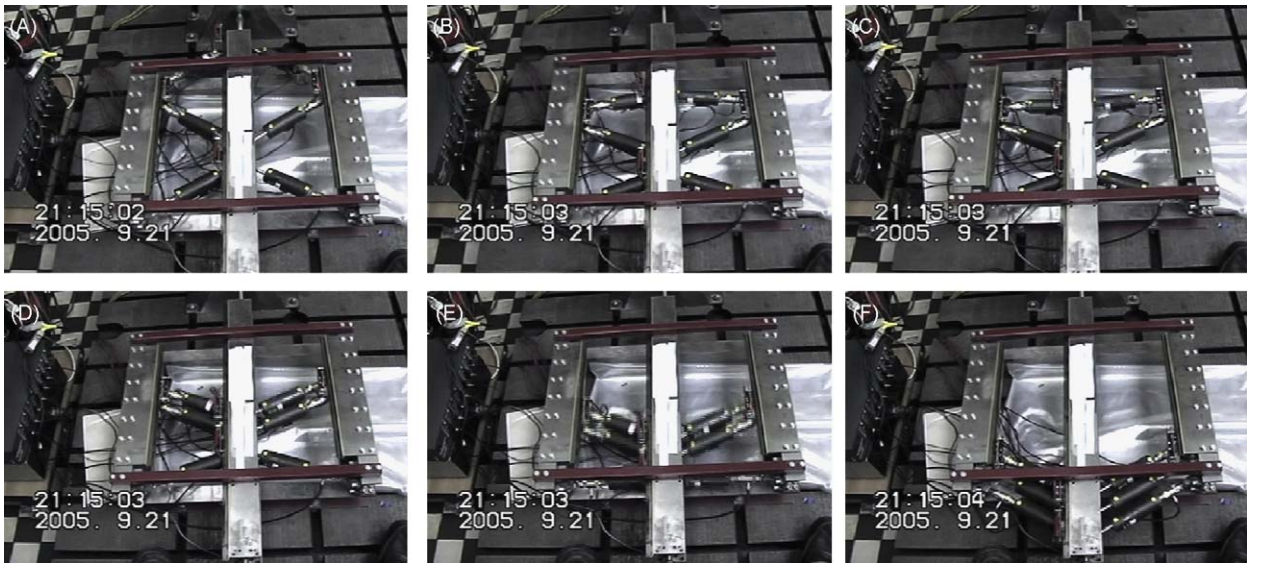

Fig. 6. Experimental behaviour showing top members initiating folding process from (A) to (F) (also shown in Ref. [11]).

3.5. *Local folding initiated by top members for* (η_1)

The behaviour shown by the truss for the top members folding is similar to the behaviour seen when the bottom members initiate the folding.

The experimental behaviour showing the top members initiating the folding process is shown in Fig. 6. The numerical solutions and folding processes using the displacement control method are shown in Fig. 7.

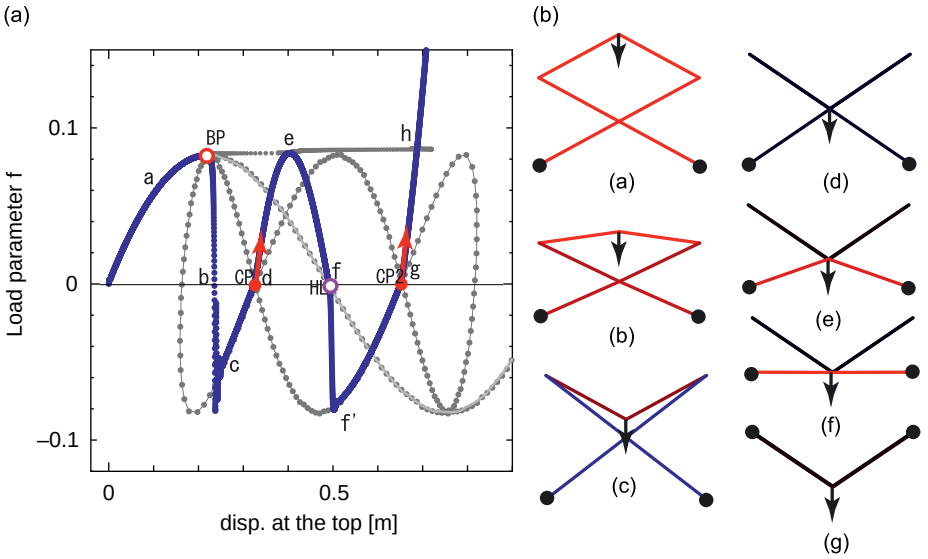

Fig. 7. Numerical results for top members initiating folding process with contact (also shown in Ref. [11]): (a) shows the dynamic equilibrium paths for both displacement controlled (shown bold) and load controlled (shown as horizontal line BP to (e) to (h)), (b) folding processes by the dynamic displacement control method. (The red colour indicates compressive stress and blue colour indicates tensile stress.) (For interpretation of the references to colour in this figure legend, the reader is referred to the web version of this article.)

The experimental behaviour is described as follows: Picture (A) in Fig. 6 shows the initial position; Picture (B) shows the top members during the first snap-through process and just prior to achieving a horizontal state; Picture (C) shows post-snap through of the top members just past horizontal; Picture (D) shows the restabilised state after the top members have undergone the snap-through process; Picture (E) shows the bottom members just about to snap through; Picture (F) shows the post-snap-through stabilised state.

For the displacement control simulation Fig. 7(a) shows at BP (i.e. the onset of instability) there is a sudden loss of stiffness and the path followed is shown as a negative load value with the blue solid line. Hence the path followed is (a)–BP–(b)–(c)–CP–(e)–(f)–(f′)–(g)–(h). After the first snap through of the top members there is local restabilisation and a positive stiffness. The line keeps climbing through (c)–(d) (or CP) until (e) is reached which marks the onset of the second instability and the bottom members snap through. The line followed here is (e)–(f)–(f′). When restabilisation occurs no further snap through is possible and the system stiffness keeps increasing starting at (f′)–(g)–(h). When compared to the static paths the dynamic processes after (d) and (g) show higher system stiffnesses. These increases occur when nodes come into contact and members are collinear and adjacent. It is observed that the path of (d)–(e)–(f) corresponds to the local equilibrium curve of a Von Mises truss model. For the load control simulation Fig. 7(a) shows the path followed as the row of horizontal gray dots. Hence the path followed is shown with two snap-throughs as BP to (e) and (e) to (h). As can be seen in the figure, point (h) corresponds to the final point after all members are in contact. When restabilisation occurs no further snap through is possible and the system stiffness keeps increasing. For the displacement control simulation the folding process is shown as (a)–(g) in Fig. 7(b). For the load control simulation the folding process is shown as BP, (e) and (h). Hence there are two snap-throughs: first in the top members and then later in the bottom members for either approach.

3.6. *Local folding initiated by middle members for* (η_2)

The experimental folding behaviour showing the middle members initiating the folding process is shown in Fig. 8. The numerical solutions and folding processes are shown in Fig. 9. The experimental behaviour is described as follows: Picture (A) in Fig. 8 shows the initial position; Picture (B) shows the middle members during the first snap-through process and just prior to achieving a horizontal state; Picture (C) shows post-snap through of the middle members just past horizontal; Picture (D) shows the restabilised state with all

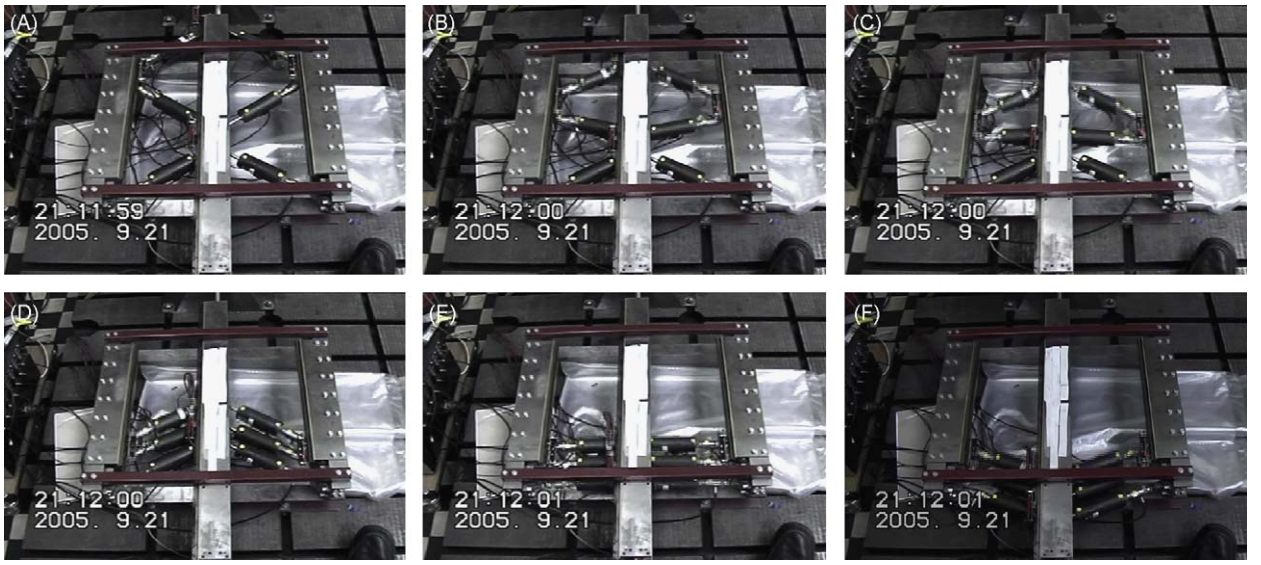

Fig. 8. Experimental behaviour showing mid members initiating folding process from (A) to (F).

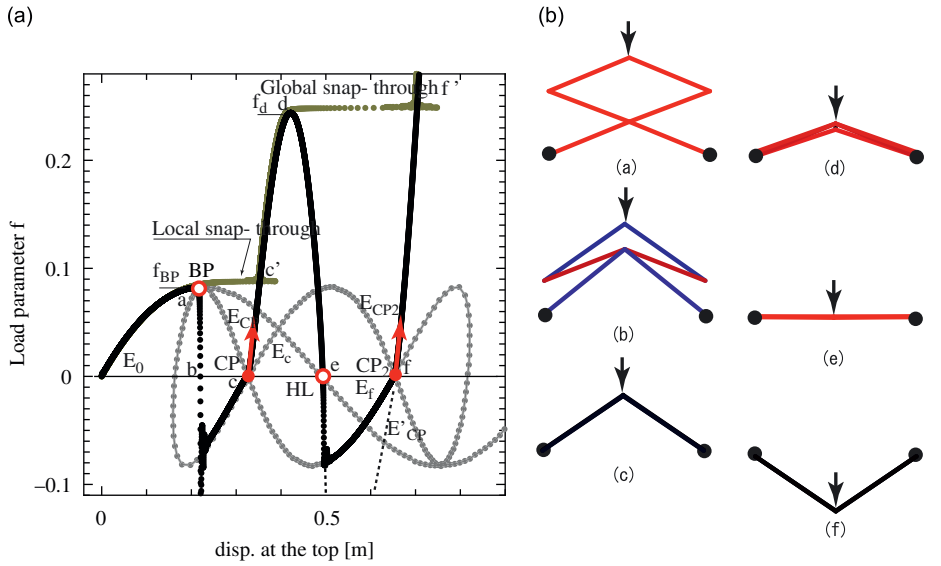

Fig. 9. Numerical results for mid members initiating folding pattern: (a) dynamic and static equilibrium paths compared, (b) folding processes by the dynamic displacement control method. (The red colour indicates compressive stress and blue colour indicates tensile stress.) (For interpretation of the references to colour in this figure legend, the reader is referred to the web version of this article.)

members collinear; Picture (E) shows all the members just about to snap through; Picture (F) shows the post-snap-through stabilised state.

For the displacement control simulation Fig. 9(a) shows at BP (i.e. the onset of instability) there is a sudden loss of stiffness and the path followed is shown as the black colour solid dots. After snap through of the middle members there is local restabilisation and a positive stiffness. The line keeps climbing through (c) until (d) is reached. The maximum load parameter for this folding pattern is larger than two previous foldings. The maximum load value is approximately three times the load parameter at BP. This is caused by a substantial increase in stiffness and a large load is required for the second snap through because three layers of the truss

need to snap through. (d) marks the onset of the second instability and all the members snap through. The line followed here is (d)–(e)–(f)–(f′). When restabilisation occurs no further snap through is possible and the system stiffness keeps increasing. When compared to the static paths the dynamic processes after (c) shows higher system stiffnesses. These increases occur when nodes come into contact and members are collinear and adjacent. For the load control simulation Fig. 9(a) shows the dynamic path followed as the row of horizontal yellow dots. Hence the path followed is shown with two snap-throughs which occur at two different levels of load parameter, i.e. as BP to (c′) and (d) to (f′). The load f_d for this pattern is almost three times the load at f_{BP}. Hence there are two snap-throughs first in the middle members and then later in all the members simultaneously for both approaches. Each point (a)–(f) on the equilibrium path in Fig. 9(a) corresponds to the folding process (a)–(f) in Fig. 9(b) for the displacement control simulation.

3.7. Comparison of the folding patterns

We have successfully obtained the numerical simulation for the folding of a multi-layered truss for both static and dynamic considerations and have numerically demonstrated the characteristics for each of the folding patterns. For the dynamic case three patterns are identified and shown in Fig. 10(a). The two dynamic paths for folding patterns 1 and 3, shown as green and orange lines, referring to top and bottom member initiated folding, are similar. The dynamic paths for the folding pattern 2 (middle member initiated folding) is noticeably different and has a substantially larger load parameter requirement for snap the second snap through. The figure also shows the static paths shown grey. The sections of the dynamic paths which follow the same paths as the static solution occurs only where there is no contact. After contact between nodes (in the dynamic problem) there is an increase in the system stiffness and the dynamic path diverges from the static paths.

Fig. 10(b) shows kinetic energy for the dynamic load control. Kinematic energy for top and bottom member initiated folding patterns are similar. It is seen that kinematic energy for folding pattern 2 is much larger due to the large increase in stiffness and hence a larger load requirement to precipitate the second snap through. The second snap through requires snap through of all members and may be considered as a global snap through (Fig. 10(b)).

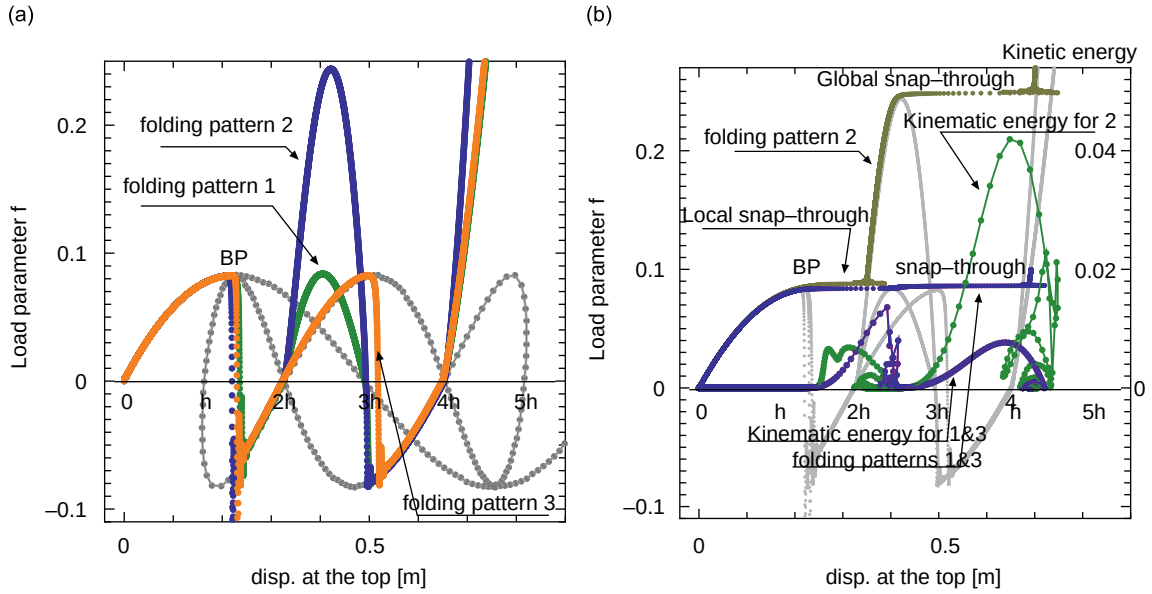

Fig. 10. Comparison of the three folding patterns where folding patterns 1, 2 and 3 correspond to top, mid and bottom members initiating folding process, respectively: (a) dynamic paths, (b) kinetic energy for dynamic load control (Note both figures show the static paths in grey.).

4. Asymmetric folding uncertainty and its effects on folding symmetry

The three local folding patterns that have been observed in the laboratory have been discussed above. There are other modes that are possible but which are difficult to observe. It has been experimentally demonstrated that it is possible for nonsymmetric modes to occur as shown in Fig. 11.

The truss system will have asymmetry if individual elements have variation in their parameters. If there is sufficient variation then it maybe possible to obtain a substantially different folding pattern such as the unsymmetrical pattern observed in Fig. 12. Here, the geometry of the system has symmetry, but there are different prestresses in the members. Although this folding pattern is mentioned—its exact causes are beyond the scope of this paper and is just to alert the reader to other possible patterns that can occur in the physical world.

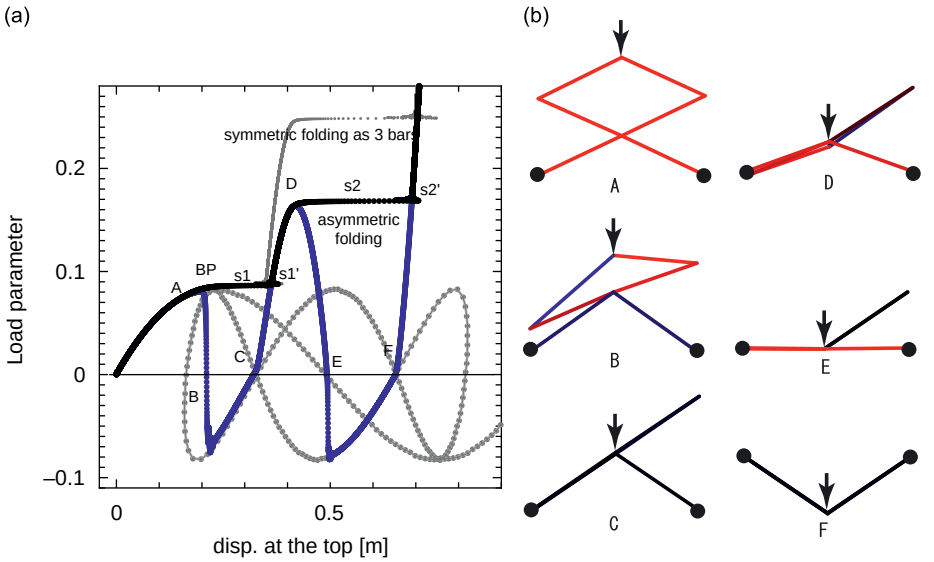

Fig. 11. Equilibrium curves for the asymmetric folding pattern.

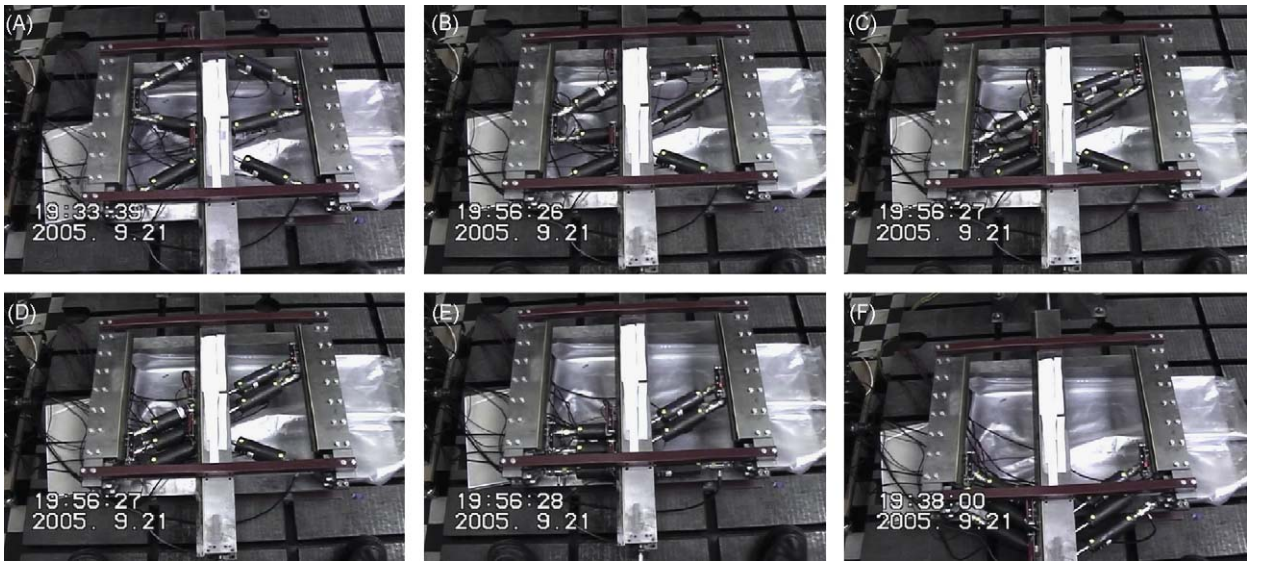

Fig. 12. The process of symmetry-breaking folding pattern.

5. Conclusion

In this paper, the nonlinear path folding behaviour of a folding truss has been analysed from a theoretical basis and by computing numerical simulations. The numerical solutions are compared to published experimental work carried out by Holnicki-Szulc et al. [9,10] in the Polish Academy of Sciences. The theoretical and numerical analyses have shown that the behaviour of the folding truss is dependent on both the velocity of a dynamic loading and the initial geometry of a structure. It has been demonstrated that there are several BP and equilibrium paths for the model which has a singular problem at *the maximum limit point* and *the multiple BP*. It has further been shown that the number and complexity of the folding patterns are a function of the number of layers in the system. Hence when there are more layers in the truss there is an increase in the folding patterns due to this larger number of degree of freedom of a model. The analyses have shown that in solving the nonlinear governing equations there are implicit and complex bifurcation paths along the unstable primary path during the folding mechanism for both the static and dynamic problems (i.e. without and with contact respectively). When allowance was made for contact between nodes and elements it was found that, for the middle folding truss, the piling bar elements substantially increase the stiffness of the truss. If changeable nonlinear stiffness (e.g. imperfection control) is applied to a deployable structure it will then be possible to control the folding pattern. For the multi-layered truss, there have been several folding mechanisms and sequential snap-through behaviours identified, both global and local foldings. The local behaviour of the truss is analogous to the micro-structure behaviour of a honeycomb material and the global behaviour of the truss is similar to the natural failure for this type of material. In summary this research has investigated the basic mechanism of the dynamic folding of a pantographic system with symmetry, based on bifurcation analysis. For other systems, such as those typified by light weight structures or cellular structure, then they may also exhibit the folding behaviour shown herein.

Acknowledgements

This work has been supported by a Grant-in-Aid for Scientific Research (C) Foundation in Japan Society for the Promotion of Science. The authors are also very grateful to Prof. J. Holnicki-Szulc of the Institute of Fundamental Technological Research, Polish Academy of Sciences for the photographs of the folding experiment carried out by Dr. P. Pawloski and his team. The authors are also very grateful to Prof. M. Nakazawa of Tohoku-Gakuin University for his help with the mathematical formulation. The authors are also very grateful for the comments from the referees of this paper.

Appendix A. Strain definition

Strain can be defined as normal strain (general engineering strain) or as Green's strain. Numerical results for the equilibrium curves have been calculated by using both definitions. In the body of the paper the authors have used Green's formulation for strain defined in Eq. (5).

Normal strain for an element i is defined in the following equation:

$$\varepsilon_i^* = \frac{\hat{\ell}_i}{\ell_i} - 1 \quad \text{for } i = 1, \ldots, m. \tag{30}$$

Total strain energy for both strain approaches are defined as

$$\mathscr{U} = \sum_{i=1}^{m} \frac{EA\ell_i}{2} (\varepsilon_i)^2 \quad \text{(Green' s strain)}, \tag{31}$$

$$\mathscr{U}^* = \sum_{i=1}^{m} \frac{EA\ell_i}{2} (\varepsilon_i^*)^2 \quad \text{(Normal strain)}. \tag{32}$$

A ratio α is now introduced where α is defined as a load ratio and is equated as $\alpha = f^*/f$, where f and f^* are the load parameters for each strain approach (where '$*$' denotes normal strain).

$$\alpha = \frac{f^*}{f} = \frac{\partial \mathscr{U}^*/\partial v_1}{\partial \mathscr{U}/\partial v_1} = \frac{\mathscr{U}^*}{\mathscr{U}} = \frac{\sum(\varepsilon_i^*)^2}{\sum(\varepsilon_i)^2}$$

$$\approx \frac{(\varepsilon_1^*)^2}{(\varepsilon_1)^2} = 4 \cdot \frac{\left(\dfrac{\hat{\ell}_1}{\ell_1} - 1\right)^2}{\left\{\left(\dfrac{\hat{\ell}_1}{\ell_1}\right)^2 - 1\right\}^2} = 4 \frac{\left(\dfrac{\sqrt{(\gamma - \bar{v}_1 + \bar{v}_2)^2 + 1}}{\sqrt{\gamma^2 + 1}} - 1\right)^2}{\left(\dfrac{(\gamma - \bar{v}_1 + \bar{v}_2)^2 + 1}{\gamma^2 + 1} - 1\right)^2}$$

$$= \frac{4(\gamma^2 + 1)(\sqrt{\gamma^2 + 1} - \sqrt{(\gamma - \bar{v}_1 + \bar{v}_2)^2 + 1})^2}{(\bar{v}_1 - \bar{v}_2)^2(2\gamma - \bar{v}_1 + \bar{v}_2)^2}. \tag{33}$$

The above equation shows the comparison between the partial strain energies ($(\varepsilon_1)^2$ and $(\varepsilon_1^*)^2$), and it is seen in Fig. 13 that the normal strain energy formulation is higher than for Green's strain formulation. (For this calculation the following parameters are used: $\bar{v}_2 = 2\bar{v}_1/3,\ h = 0.163,\ L = 0.24,\ EA = 1$.)

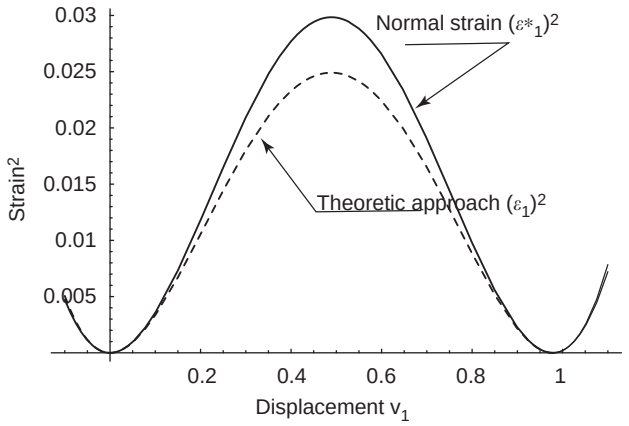

Fig. 13. Graph showing the different values of the squares of strain caused by using normal strain and Green's strain.

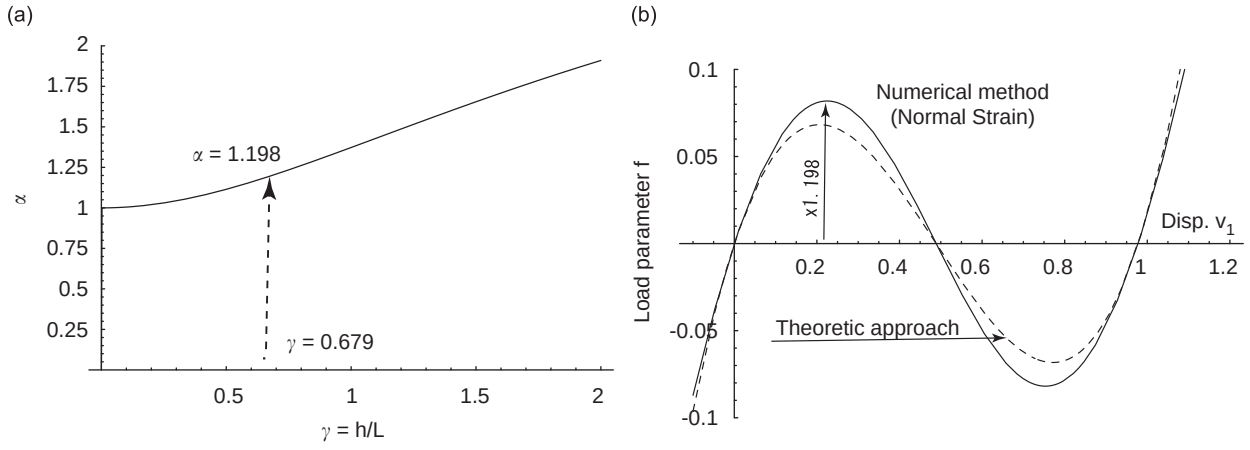

Fig. 14. A comparison of using the two different strain formulations—normal strain and Green's strain: (a) the relationship between γ and α showing that the shallower arch has a load ratio α close to unity, (b) primary equilibrium paths for both strain formulations.

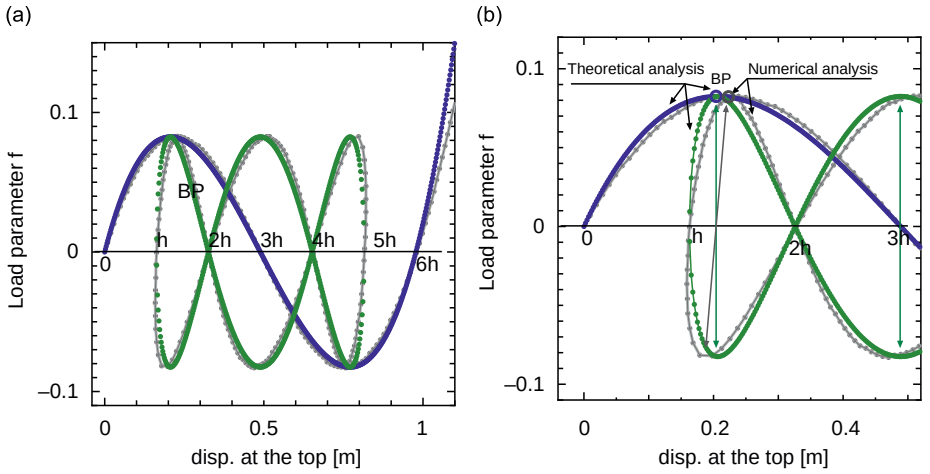

Fig. 15. Equilibrium paths: green/blue paths obtained using Green's strain and grey paths obtained with normal strain (For interpretation of the references to colour in this figure legend, the reader is referred to the web version of this article.).

If the snap-through behaviour for one layer is considered then $\bar{v}_2 = 0$ and $\bar{v}_1 = \gamma$; the critical value for α is then given as

$$\alpha \approx \frac{f^*}{f} = \frac{4(1+\gamma^2)(2+\gamma^2-2\sqrt{1+\gamma^2})}{\gamma^4}. \tag{34}$$

This ratio of the load parameters is a function of the aspect ratio γ only. The relationship between α and γ is shown in Fig. 14(a). When γ is 0.679 (i.e. 0.163 m/0.24 m), the ratio $\alpha = 1.198$.

For the multiple lay truss, using the same numerical conditions ($v_2 = 2v_1/3,\ h = 0.163,\ L = 0.24,\ EA = 1$), the numerical results for the primary equilibrium path are shown in Fig. 14(b).

Finally, it is shown in Fig. 15, the static paths and the primary path for both strain approaches. The grey line shows the numerical result based on the definition of normal strain; the blue and green lines show the Green strain formulation results. The bifurcation path of grey line (normal strain) has skewed a small amount. The green line has symmetry about the horizontal axis.

Appendix B. Equilibrium formulation of three layers truss

The equilibrium equations for the 3 bar truss have been obtained from Eqs. (11)–(13) as follows:

$$F_1 = \frac{\beta}{2}(\bar{v}_1-\bar{v}_2)\{(\bar{v}_1-\bar{v}_2)-\gamma\}\{(\bar{v}_1-\bar{v}_2)-2\gamma\} - \frac{f}{2} = 0, \tag{35}$$

$$\begin{aligned} F_2 = & -(\bar{v}_1-\bar{v}_2)\{(\bar{v}_1-\bar{v}_2)-\gamma\}\{(\bar{v}_1-\bar{v}_2)-2\gamma\} \\ & +(\bar{v}_2-\bar{v}_3)\{(\bar{v}_2-\bar{v}_3)-\gamma\}\{(\bar{v}_2-\bar{v}_3)-2\gamma\} = 0, \end{aligned} \tag{36}$$

$$F_3 = -(\bar{v}_2-\bar{v}_3)\{(\bar{v}_2-\bar{v}_3)-\gamma\}\{(\bar{v}_2-\bar{v}_3)-2\gamma\} + \bar{v}_3(\bar{v}_3-\gamma)(\bar{v}_3-2\gamma) = 0. \tag{37}$$

Rearrangement of Eq. (37) gives

$$(2\bar{v}_3-\bar{v}_2)(\bar{v}_3^2-\bar{v}_2\bar{v}_3+\bar{v}_2^2-3\gamma\bar{v}_2+2\gamma^2) = 0.$$

Then, the relationship between $\bar{v}_3$ and $\bar{v}_2$ is obtained as

$$\bar{v}_3 \begin{cases} = \bar{v}_2/2, \\ = \frac{1}{2}(\bar{v}_2 \pm \sqrt{-3\bar{v}_2^2+12\gamma\bar{v}_2-8\gamma^2}). \end{cases} \tag{38}$$

If we adopt the first equality of Eq. (38) i.e. $(\bar{v}_2-\bar{v}_3)=\bar{v}_2/2$ and substitute it into Eq. (36), we obtain the relation between $\bar{v}_2$ and $\bar{v}_1$ as

$$-(\bar{v}_1-\bar{v}_2)\{(\bar{v}_1-\bar{v}_2)-\gamma\}\{(\bar{v}_1-\bar{v}_2)-2\gamma\}+\frac{\bar{v}_2}{2}\left(\frac{\bar{v}_2}{2}-\gamma\right)\left(\frac{\bar{v}_2}{2}-2\gamma\right)=0,$$

$$\left(\frac{3}{2}\bar{v}_2-\bar{v}_1\right)\left\{\frac{3}{4}\bar{v}_2^2-\frac{3}{2}\bar{v}_1\bar{v}_2+\bar{v}_1^2-3\gamma\left(\bar{v}_1-\frac{\bar{v}_2}{2}\right)+2\gamma^2\right\}=0, \tag{39}$$

$$\bar{v}_2\begin{cases}=\frac{2}{3}\bar{v}_1,\\ =(-\gamma+\bar{v}_1)\pm\frac{\sqrt{3}}{3}\sqrt{-(\bar{v}_1-\gamma)(\bar{v}_1-5\gamma)}.\end{cases} \tag{40}$$

Moreover, in order to obtain the relationship between the load f and $\bar{v}_1$, we substitute Eq. (40) into Eq. (35). Adopting the relationship $\bar{v}_2=2\bar{v}_1/3$, i.e. $(\bar{v}_1-\bar{v}_2)=\bar{v}_1/3$ results in the following:

$$f_{\text{pri.}}=\beta\frac{\bar{v}_1}{3}\left(\frac{\bar{v}_1}{3}-\gamma\right)\left(\frac{\bar{v}_1}{3}-2\gamma\right). \tag{41}$$

This equation is for the primary path (i.e. proportional displacement hence $(\bar{v}_1-\bar{v}_2)=(\bar{v}_2-\bar{v}_3)=\bar{v}_1/3$).

Adopting Eq. (40), i.e. $(\bar{v}_1-\bar{v}_2)=\gamma\mp Q$, where $Q=\frac{\sqrt{3}}{3}\sqrt{-(\bar{v}_1-\gamma)(\bar{v}_1-5\gamma)}$ results in the following equation:

$$f_{\text{bif.}}=\beta(\gamma\mp Q)(\mp Q)(-\gamma\mp Q),$$

therefore

$$f_{\text{bif.}}=\pm\frac{\beta}{3\sqrt{3}}(\bar{v}_1-2\gamma)(\bar{v}_1-4\gamma)\sqrt{-(\bar{v}_1-\gamma)(\bar{v}_1-5\gamma)}. \tag{42}$$

Therefore, Eqs. (41) and (42) correspond to Eqs. (23) and (24), respectively.

References

[1] J.M.T. Thompson, G.W. Hunt, *A General Theory of Elastic Stability*, Wiley, London, 1973.

[2] G.W. Hunt, G. Baker, Principles of localization in the fracture of quasi-brittle structures, *Journal of the Mechanics and Physics of Solids* 43 (7) (1995) 1127–1150.

[3] K. Ikeda, P. Providencia, G.W. Hunt, Multiple equilibria for unlinked and weakly-linked cellular structural forms, *International Journal of Solids and Structures* 30 (3) (1993) 371–384.

[4] J.S. Humphreys, S.R. Bodner, Dynamic buckling of shallow shells under impulsive loading, *Journal of the Engineering Mechanics Division, Proceedings of the ASCE* 88 (2) (1962) 17–36.

[5] W. Nachbar, N.C. Huang, Dynamic snap-through of a simple viscoelastic truss, *Quarterly of Applied Mathematics* 25 (1967) 65–82.

[6] N.C. Huang, Axisymmetric dynamic snap-through of elastic clamped shallow spherical shells, *AIAA Journal* 7 (2) (1969) 215–220.

[7] I. Ario, Homoclinic bifurcation and chaos attractor in elastic two-bar truss, *International Journal of Non-Linear Mechanics* 39 (4) (2004) 605–617.

[8] G.W. Hunt, M.A. Peletier, A.R. Champneys, P.D. Woods, M. Ahmer Wadee, C.J. Budd, G.J. Lord, Cellular buckling in long structures, *Nonlinear Dynamics* 21 (1) (2000) 3–29.

[9] J. Holnicki-Szulc, P. Pawlowski, M. Wiklo, High-performance impact absorbing materials—the concept, design tools and applications, *Smart Materials and Structures* 12 (2003) 461–467.

[10] J. Holnicki-Szulc, P. Pawłowski, The concept of multifolding and its experimental validation, *Proceedings of XXI ICTAM, Warsaw*, 2004.

[11] I. Ario, A. Watson, Dynamic folding analysis for multi-folding structures under impact loading, *International Journal of Sound and Vibration* 308 (3–5) (2007) 591–598.

[12] K. Ikeda, K. Murota, Bifurcation hierarchy of symmetric structures, *International Journal of Solids and Structures* 27 (12) (1991) 1551–1573.

[13] M.A. Crisfield, Snap-through and snap-back response in concrete structures and the dangers of under integration, *International Journal for Numerical Methods in Engineering* 22 (3) (1986) 751–767.

[14] E. Riks, An incremental approach to the solution of snapping and buckling problems, *International Journal of Solids and Structures* 15 (1979) 524–551.

[15] J.L. Batoz, G. Dhatt, Incremental displacement algorithms for nonlinear problems, *International Journal for Numerical Methods in Engineering* 14 (1979) 1262–1267.
[16] M.A. Crisfield, A fast incremental/iterative solution procedure that handles "snap-through," *Computers & Structures* 13 (1981) 55–62.
[17] P.X. Bellini, A. Chulya, Improved automatic incremental algorithm for the efficient solution of nonlinear finite element equations, *Computers & Structures* 26 (1–2) (1987) 99–110.
[18] M.A. Crisfield, Arc-length method including line searches and accelerations, *International Journal for Numerical Methods in Engineering* 19 (9) (1983) 1269–1289.